Spatial bistability and excitability in the chlorite-tetrathionate reaction in cylindrical and conical geometries

D. E. Strier and J. Boissonade*
Centre de Recherche Paul Pascal (CNRS), Av. Schweitzer, F-33600 Pessac, France
(Received 8 March 2004; published 23 July 2004)

Spatial bistability and excitability in the chlorite-tetrathionate reaction, performed in gels fed by diffusion from one boundary, have been extensively studied, both experimentally and numerically, in a flat annular striplike geometry. We first complement these numerical results. Afterwards, we extend the calculations to the cylindrical and conical geometries. In the cylinder, we compute the limits of bistability and of excitability which are important for experiments in chemomechanics but cannot be directly measured. The results of the simulations in the conical geometry agree with previous experiments on the corresponding setup. We show that the characteristics of the traveling waves which spontaneously arise in the latter geometry provide a simple and direct experimental access to these limits.

DOI: 10.1103/PhysRevE.70.016210 PACS number(s): 82.40.Bj, 82.40.Ck, 82.33.Ln, 05.45.−a

I. INTRODUCTION

The chlorite-tetrathionate reaction (hereafter referred as CT) has become a prototype in the study of several classes of reaction-diffusion instabilities and dissipative structures in chemical systems far from equilibrium. When the reaction is achieved within an inert hydrogel in order to inhibit convection, it exhibits remarkable dynamical phenomena including front instabilities [1–3], spatial bistability [4], and long range activation effects [5]. In the absence of a gel, reaction-diffusion-convection front instabilities have also been studied [6,7]. When the inert gel is replaced by a chemoresponsive gel, spontaneous changes of size and shape of this gel were experimentally observed and explained on the basis of heuristic arguments [8]. In the study of chemical patterns, it is advisable to permanently sustain stationary nonequilibrium conditions. For this purpose, it has become common to use one sided fed reactors (OSFRs). They are made up of a piece of gel, with a boundary kept in contact with the contents of a continuous stirred tank reactor (CSTR) which is maintained in a stationary state by the permanent flow of chemicals. Within the gel, the feeding of fresh reactants is achieved by diffusion from this boundary. Such OSFR's have been previously used for experiments on traveling waves [9,10], Turing patterns [11], spot splitting [12], chemical fronts digitation [13], and spatial bistability [14].

In the experiments of Refs. [4,5,8], the CT reaction was in fact operated in such reactors. Since the feeding of fresh reactants results from the diffusive transport from the boundaries, the distribution of concentrations within the gel not only depends on the concentrations in the CSTR, but also on the size and the geometry of this gel. Most of the systematic experimental studies of the CT in inert gels were worked out in a flat quasi-two-dimensional annular piece of gel fed along the external rim. This is a standard and very convenient geometry to observe the distribution of concentrations as a function of the distance to the boundaries [4,5], but, in experiments on chemomechanics, a cylindrical gel was used [8]. In order to put in evidence the key role that the size of the gel exerts on dynamical behavior, experiments with inert gels were also performed in a conical geometry [15]. Moreover, this particular geometry allows to access to properties at small sizes, which for practical reasons could not be reached otherwise. This system was found to exhibit a spontaneous nonstationary behavior and give rise to traveling waves close to the tip of the cone. Unfortunately, in these axial geometries, the distribution of concentrations along the radial direction, which governs the dynamics, cannot be accessed directly. In a previous work, it was shown that, in spite of the system complexity, numerical modeling can reproduce quantitatively the main dynamical features in the flat ring case [5]. In this paper, we shall first complement the numerical work in this standard case. Then, we shall extend the results to a cylindrical gel in order to quantitatively estimate the changes brought by this geometry. The simulations are further extended to the conical geometry and we discuss the emergence of the spontaneous traveling waves as observed in the experiments.

In excess of chlorite, the kinetics of the CT reaction is well approximated by the following overall balance equation:

$$7\ ClO_2^- + 2\ S_4O_6^{2-} + 6\ H_2O \rightarrow 7\ Cl^- + 8\ SO_4^{2-} + 12\ H^+ \tag{1}$$

the reaction rate of which is given by [16]:

$$v_R = -\frac{1}{7}\frac{d[ClO_2^-]}{dt} = k[ClO_2^-][S_4O_6^{2-}][H^+]^2. \tag{2}$$

The reaction is strongly autocatalytic in H^+. Thus, in slightly acid conditions, the reaction starts immediately, the level of H^+ increases rapidly, still increasing the reaction rate, so that the transformation is completed within a short time. On the contrary, in alcaline conditions, this reaction rate is so low that no transformation occurs within a typical experimental duration. Thus, if the input reactants are flowed into a CSTR in alcaline conditions, no reaction will take place provided

*Electronic address: boisson@crpp-bordeaux.cnrs.fr

the initial contents are not acid. In the rest of the paper, we shall assume that these conditions are fulfilled in the CSTR. Let us now assume that a small piece of gel is kept in contact with the contents of the CSTR. The volume of the CSTR is supposed to be large enough for these contents not to be significantly affected by the state of the gel, so that an alcaline state is maintained along the contact boundary. If the gel contents are also initially alcaline, no reaction occurs within the gel and the asymptotic composition will become identical to the composition in the CSTR. This will be referred as the "Flow" (or F) state. But, if the initial composition in the gel is acid, the reaction rate is strongly increased by the autocatalysis. Then, the reaction processes counterbalance the diffusion so that the gel remains acid except within a narrow boundary layer that connects the acid bulk to the alcaline boundary. This will be referred to as the "mixed" state or FT state. The "FT" name is an historical notation where the "T" stands for the "thermodynamic" state that refers to the equilibrium composition that would be asymptotically achieved in a closed system. Of course, if the gel "depth,"—i.e., the size in the directions orthogonal to the feeding boundaries —is too small (typically smaller than the boundary layer depth), this FT state cannot be sustained, since the reaction rate become smaller that the rate of the diffusive exchanges with the CSTR. Thus, provided that the gel depth is large enough, two different distributions of concentrations, namely, F and FT, are stable for the same composition in the CSTR inside a domain of parameters which depends both on the "depth" and the feeding composition. This phenomenon —here explained in the case of the CT reaction but which is quite generic for "clock reactions" exhibiting bistability in a CSTR —is referred to as "spatial bistability" and has been extensively studied in the chlorine-dioxide-iodide reaction [14], the CT reaction [4,5], and in toy models [17–20]. For a more comprehensive theory, see Ref. [14].

In addition, the CT reaction exhibits another specific behavior. The autocatalytic species H^+ diffuses much faster than the reagents $S_4O_6^{2-}$ and ClO_2^-, so that there are two antagonistic effects: on one hand, an acid perturbation tends to propagate faster, on the other hand, the exchange rates between the gel and the CSTR are higher for H^+ than for the substrates $S_4O_6^{2-}$ and ClO_2^-. This interplay, due to the long range activation, eventually leads to singular dynamics. When the *p*H in the CSTR is increased, the FT state becomes unstable at the limit of the F/FT bistability domain, but still remains excitable over a large range of this control parameter. By excitability, we mean that a small local perturbation applied to a stationary stable state rapidly increases by a large amount before the stable solution is recovered. Under the effect of diffusion, the perturbation gives rises to a pulse which propagates without deformation at constant velocity in the stable state [21,22]. Here, a local acid perturbation induces a pulse of FT state that propagates at constant shape and constant velocity within the stable state F [4,5]. Since, in this case, these traveling waves originate in the differential diffusive feeding process, they also depend on the depth of the gel. Moreover, inside the bistability domain, but just before the FT→T transition, the FT state exhibits oscillations of the boundary layer thickness, although the reaction can never be oscillating in homogeneous conditions.

In order to properly model the kinetics, it was shown [5] that the fast equilibrium

$$H^+ + OH^- \rightleftharpoons H_2O \tag{3}$$

had to be taken into account. In regard to the *p*H of the acid state in the experiments, the equilibrium

$$H^+ + SO_4^{2-} \rightleftharpoons HSO_4^- \tag{4}$$

was also retained. The rate laws of these equilibria are, respectively,

$$v_e = k_e^+ - k_e^-[H^+][OH^-], \tag{5}$$

$$v_a = k_a^+[HSO_4^-] - k_a^-[H^+][SO_4^{2-}]. \tag{6}$$

With Eq. (2) this set of equations defines a six-variable model.

The coupled dynamical equations for the concentrations in the CSTR and in the gel are, respectively,

$$\frac{\partial c_{ih}}{\partial t} = f_i(\mathbf{c}_h) + \frac{(c_{i0} - c_{ih})}{\tau} + G_i \tag{7}$$

and

$$\frac{\partial c_i}{\partial t} = f_i(\mathbf{c}) + D_i \nabla^2 c_i, \tag{8}$$

where c_{i0}, c_{ih}, and c_i are the concentrations of species i, respectively, in the input flow, in the CSTR, and inside the gel, D_i is the corresponding diffusion coefficient, τ is the residence time of the CSTR, and the f_i's are the reaction rates given by Eqs. (2)–(4). In the right-hand side of Eq. (7), the three terms represent the change of the concentrations per time unit. The first term gives the contribution of the reaction. The second one represents the input and output flows of the species. It contains all the expandable control parameters of the system, namely, τ and the c_{i0}. The third one represents the feedback of the gel contents on the CSTR and is proportional to the diffusion flow of the species through the surface of contact. It was previously shown [14] that, since the volume of the reactor is large in regard to the gel volume, this term can be neglected, specially in the pararameter domain on which we shall focus. Thus, in the following, we shall assume $G_i = 0$, so that Eq. (7) can be solved independently to provide a Dirichlet boundary condition for Eq. (8).

In all computations, we shall fix the residence time of the CSTR to $\tau = 600$ s, the concentrations in the input flow to $[ClO_2^-]_0 = 1.9 \times 10^{-2}$ M, $[S_4O_6^{2-}]_0 = 0.5 \times 10^{-2}$ M, and the kinetic constants to $k = 5 \times 10^6$ M^{-3} s^{-1}, $k_e^- = 1.4 \times 10^{11}$ M s^{-1}, $k_e^+ = K_e\, k_e^-$ with $K_e = 10^{-14}$, $k_a^- = 10^{11}$ M s^{-1}, $k_a^+ = K_a\, k_a^-$ with $pK_a = -\log(K_a) = 1.94$ like in Refs. [4,5]. The choice of diffusion coefficients raises a problem: whereas the autodiffusion coefficients of H^+ and OH^- are much larger than those of the other ionic species, the condition of local electroneutrality tends to smooth these differences. Therefore, all the diffusion coefficients will be fixed in an heuristic way to a standard value $D = 10^{-5}$ cm^2 s^{-1} except those of the fast species that will be both fixed to $D_{H^+} = D_{OH^-} = 3.4 \times 10^{-5}$ cm^2 s^{-1}. In spite of its apparent crudeness, this approximation was previously found to best fit the experimental data of Refs. [4,5].

FIG. 1. Pulse of H^+ propagating to the right within the stable alcaline F state (grey scale: minimum black, maximum white). The CSTR is located at the bottom, the impermeable wall at the top. Strip width: $l=0.5$ mm, $[OH^-]_0=1.093\times10^{-2}$ M.

We have investigated three different geometries, namely, the flat strip which models the experiments of Refs. [4,5], the cylinder used in experiments on chemomechanics [8], and the cone which models the experiments of Ref. [15]. Like in the latter reference, we shall express the control parameter in terms of the concentration $[OH^-]_0$ in the total input flow rather than the equivalent operational parameter α, used in the previous publications, since the physical meaning of α is less evident in a theoretical context.

II. FLAT STRIP

In the experiments, the reactor was made of a flat annular piece of gel. The outer rim —of radius R_{ext}—is kept in contact with the CSTR and the inner rim —of radius R_{in}—is pressed against an impermeable wall. The film thickness is small enough for the system to be considered as two-dimensional. Given that the "depth" $l=R_{ext}-R_{in}$, is small in regard to these radii ($l\ll R_{in}\sim R_{ext}$), the effects of the curvature on the dynamics can be neglected. For the system to be effectively considered as two-dimensional, l must be significantly larger than the thickness of the gel film. Since, for technical reasons, such as mechanical cohesion, this thickness cannot be decreased below a minimum value (typically 0.5 mm), this constitutes an experimental limit for l in this geometry, but this limit can be numerically surpassed. In the numerical simulations the system is treated as a long rectangular strip of width l. The nonequilibrium phase diagram is built in the parameter plane ($[OH^-]_0$, l): This diagram exhibits the changes in the bistability, oscillations, and excitability domains with the width l of the strip.

The solutions of Eqs. (7) and (8) are obtained by finite differences algorithms for stiff systems. To determine with precision the limits of the spatial bistability and oscillatory domains, only one-dimensional calculations in the direction orthogonal to the faces are necessary. This was already achieved in Ref. [5]. In addition, we report here the limits of the excitability domain, which needed full two-dimensional computations with a backward implicit algorithm for stiff systems. In Fig. 1, we give an example of an acid pulse propagating within the stable alcaline state. The previously computed domains and the new computed excitability limits are gathered in Fig. 2. The horizontal double arrows indicate the corresponding experimental domains that had been investigated. Note that the experimental data at $l=0.5$ mm are highly uncertain, in particular the limit of the excitability domain since the number of experimental points is reduced due to the technical limitations mentioned above. As expected, at very small l, the alcaline F state always invades the gel so that both bistability and excitability disappear.

In spite of the apparent crudeness of the model and the strong approximations in the diffusion coefficients, the results are in quasiquantitative agreement and make us confident that these results are valid in regions where the computed limits or the state determination are yet experimentally inaccessible.

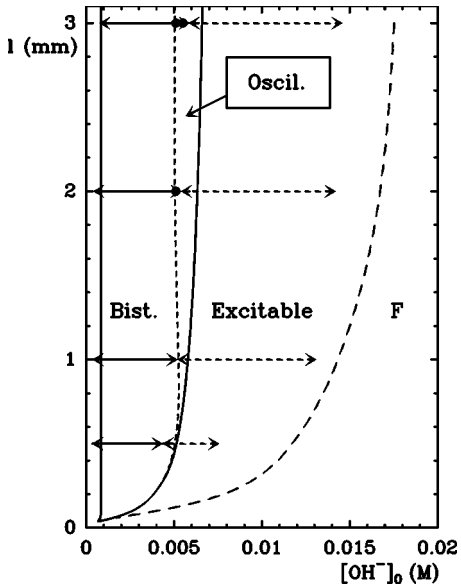

FIG. 2. Non equilibrium phase diagram in the strip geometry. Full curves: bistability limits. Dashed lines: excitability limits (long dashes), oscillations limits (short dashes). Double arrows: experimental extent of bistability domain (full arrow) and excitability domains (dashed arrow) from [4,5]. Bullets: experimental oscillations.

III. CYLINDRICAL GEOMETRY

In experiments, the distribution of concentrations is characterized by a color indicator. So, when the piece of gel is cylindrical, it is impossible to make a direct observation of this distribution in the "depth" of the gel, i.e., along a radius, since the light intensity is integrated across the gel. Only the states in the axial direction can be differentiated. Nevertheless, the radial distribution can be computed on the same lines as precedently. Assuming that there is no instability which breaks the axial symmetry, Eq. (8) is solved in cylindrical coordinates, using

$$\nabla^2 c=\frac{\partial c}{\partial r}+\frac{1}{r}\frac{\partial^2 c}{\partial r^2}+\frac{\partial^2 c}{\partial z^2}, \tag{9}$$

where r is the radial coordinate and z the coordinate along the axis. We have only searched the position of the FT→F transition and the limit of the excitability domain. When the gradient of concentration in the radial direction is constant, the diffusion flow exchanged through a given shell increases with the distance to the axis. Thus, although the radius R of the cylinder plays a role analog to l in the flat strip, external shells are favored in regard to the inner core so that the state F should be more favored than in the flat strip. Computations of the FT→F transition position are performed in one dimension since it is associated to the dynamics in the sole radial direction ($z=$Const). For the excitability limits, full two dimensional calculations are again necessary, since the

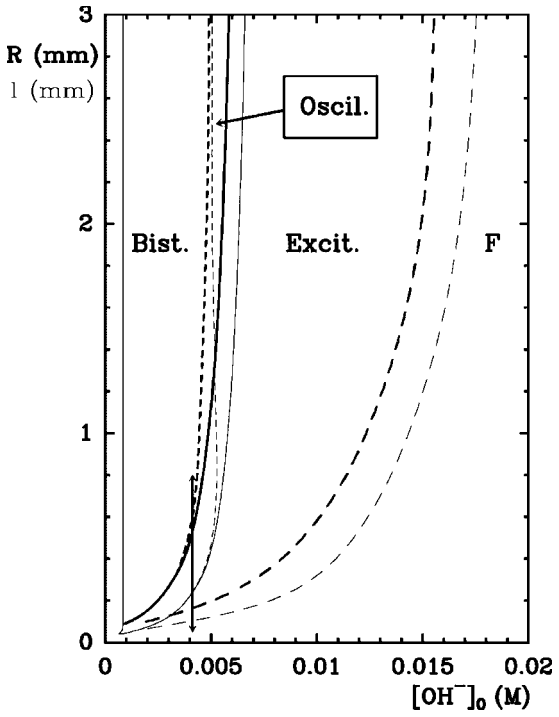

FIG. 3. Nonequilibrium phase diagram in the cylindrical geometry. Full curves: bistability limits; Short dashes: oscillations limits; long dashes: excitability limits. Thin curves correspond to the limits in the rectangular strip geometry (see Fig. 2). The vertical double arrow will be defined in the next section.

acid pulse propagates along the cylinder axis direction.

In Fig. 3, we have reported the computed limits of the different domains for the cylindrical geometry (thick curves) in the plane $([OH^-]_0, R)$. In order to make the comparison easier, the same previous limits obtained for the flat strip are also shown in the figure (thin curves) taking l in place of R. Both diagrams are similar. As expected, the limits are slightly shifted to the left, i.e., for the same values of the size R and l, the FT state cannot be sustained at $[OH^-]_0$ values as large as in the flat strip case. Accordingly, at a given value of $[OH^-]_0$, the minimal value of R that allows to sustain this FT state is larger than the corresponding minimal value of l. The features of the oscillations are similar to those of the flat strip system. Like in this flat strip, we have also observed period doubling sequences (not reported here) close to the limit of the oscillatory domain like in Ref. [5]. Nevertheless, the oscillatory region is significantly narrower than in the strip geometry, which can be understood in the following way. Oscillations come out when the position of the front which corresponds to the transition between the acid and the alcaline part of the gel in the FT state becomes unstable. In the strip geometry, this occurs when this front comes close to the impermeable wall, more precisely, when the alcaline boundary layer becomes of the same order as the depth l. In the cylindrical geometry, the role of the wall is reduced to the sole axis, so that the extent of the domain where the front "feels" the wall is much smaller.

Although no direct experimental data could be obtained in the cylinder case, our results allow to evaluate the corrections to bring to the data obtained in the strip case.

IV. CONICAL GEOMETRY

Although it is very difficult to prepare series of well calibrated cylindrical gels at small radii, it is less demanding to prepare a unique sample of a conical gel. This sample covers a large continuous range of radii at the same time, but the more complex dynamics that this geometry generates [15] has to be linked to the previous results.

Let us now consider a conical piece of gel, where ρ is the distance to the top and θ_0 is the top angle taken from the axis. If $\theta_0 \ll 1$, the cone can be considered locally as a cylinder, the radius of which is slowly changing along the axis according to $r \simeq \rho\theta_0$. Thus, in the absence of diffusion along the axis, the local dynamical properties would approximatively correspond to those along a vertical segment in the cylinder diagram in Fig. 3. The purpose of our calculations is to show how this diffusion can control global dynamics. We shall show that, according to this dynamical behavior, experimentalists can take advantage of this particular geometry, either to access simultaneously to some of the limits in Fig. 3 in a one shot experiment, either to induce spontaneous relaxation oscillations of large amplitude.

We again assume that the axial symmetry is not broken by the dynamics. Therefore, in Eq. (8), the Laplacian in spherical coordinates becomes

$$\nabla^2 c = \frac{1}{\rho^2}\frac{\partial}{\partial r}\left(\rho^2 \frac{\partial c}{\partial \rho}\right) + \frac{1}{\rho^2 \sin\theta}\frac{\partial}{\partial \theta}\left(\sin\theta \frac{\partial c}{\partial \theta}\right). \quad (10)$$

In experiments, the cone was immersed in the CSTR, except the base which was glued to an impermeable wall. The tip is never well defined and is more or less rounded. Nevertheless, this part of the cone, where the distances to the feeding boundaries are very small, always remains in the stationary state F, whatever the exact shape of the tip is. In our computations, we shall actually consider a piece of cone defined by $\rho_{\min} \leqslant \rho \leqslant \rho_{\max}$. In order to closely simulate the experimental conditions, the external boundaries (i.e., $\theta = \theta_0$ or $\rho = \rho_{\min}$) are kept at the CSTR values, and no flux boundary conditions are applied at $\rho = \rho_{\max}$. We shall fix the angle at the top of the cone to $\theta_0 = 0.125$, of the same order of magnitude as in experiments of Ref. [15]. We only report in details the results for a typical case, namely, for $[OH^-]_0 = 4.133 \times 10^{-3}$ M. Our truncated cone is delimited by $\rho_{\min} = 0.4$ mm and $\rho_{\max} = 6.4$ mm. According to $r = \rho\theta_0$, the corresponding range of cylinder radii is $[0.05\ \text{mm}, 0.8\ \text{mm}]$ and is represented in Fig. 3 as a thin double vertical arrow. Along this curve, the limits of excitability, bistability, and oscillations are, respectively, given by $r_E = 0.14$ mm, $r_B = 0.54$ mm, $r_O = 0.61$ mm and the corresponding positions in the cone by $\rho_E = 1.12$ mm, $\rho_B = 4.32$ mm, and $\rho_O = 4.88$ mm. In Fig. 5, to allow for easy comparison, these values are reported on the ρ axis when it was found appropriate.

The system is initially in the F alcaline state everywhere. An acid perturbation is applied in the bistable or excitable domain part of the cone. After a short transient, a regime of periodic oscillations is established in the gel. A series of snapshots of the distribution of $[H^+]$ within the cone over one period is given in Fig. 4. In Fig. 5(a), we show the $[H^+]$ profiles along the axis of the cone for the same snapshots. A

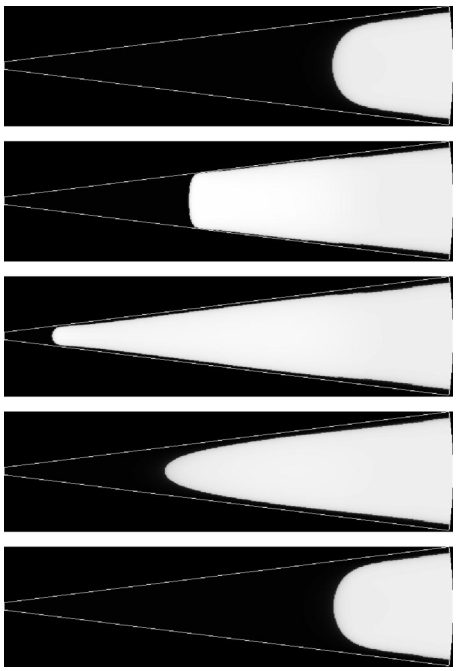

FIG. 4. Evolution of $[H^+]$ in an axial section of the cone over one period of oscillation. Parameters $[OH^-]_0=4.133\times10^{-3}$ M, $\rho_{min}=0.4$ mm, $\rho_{max}=0.64$ mm, $\theta_0=0.125$ rad. For better readablity a grey scale proportional to the logarithm of concentration is used: From $[H^+]=2.\times10^{-12}$ M (black) to $[H^+]=1.44\times10^{-2}$ M (white). Extra white lines indicate the borders of the cone. Times are counted from the begining of a period. From top to bottom: 0 s; 20 s; 32 s; 50 s; 246 s.

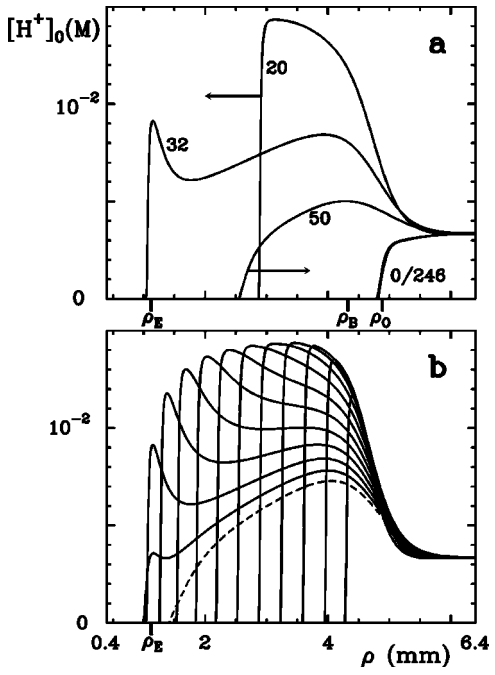

FIG. 5. Evolution of the $[H^+]$ profile along the axis of the cone during a period. Same parameters as in Fig. 4. (a) Full period: The $[H^+]$ profiles correspond to the images of Fig. 4 and are indexed with time. The arrows give the direction of motion. Labels ρ_E, ρ_B, and ρ_O correspond, respectively, to the excitability limit, the bistability limit, and the oscillations limit in the cylinder diagram of Fig. 3 for the same value of $[OH^-]_0$. (b) Successive snapshots of the $[H^+]$ profiles taken every 2 s from $t=12$ s to $t=36$ s. The front moves to the left except the last one ($t=36$ s, dashed curve).

front of acidity propagates back and forth with a period $T=246$ s. The direction of propagation changes at $t\simeq0$ s, $t\simeq32$ s, and $t\simeq246$ s. The propagation to the left (small ρ) is much faster than the propagation to the right. A sequence of axial $[H^+]$ profiles during this sole rapid phase is shown in Fig. 5(b) with a shorter sampling time than in Fig. 5(a).

Let us now describe and interpret the motions of the F/FT interface in the axial direction starting from $t=0$. Within the bistability region, the F state and the FT are both stable. Nevertheless, as a consequence of long range activation, if these two states are in contact, the FT state always propagates into the F state and invades the system [5]. Since the induction time of the reaction is quasi-infinite, an acid perturbation is necessary to initiate the FT state, but, afterwards, at large ρ, the gel always remains in the FT state. Slightly beyond the bistability limit, the FT state is no longer stable but an acid perturbation propagates under the form of a localized pulse. This defines the excitability domain. In the cone, the FT state at large ρ creates the acid perturbation which initiates the pulse and propagates to the left [Fig. 5(b)] up to the limit of the excitability domain, i.e., at $\rho=\rho_E$. One could expect that the pulse would propagate with damping beyond this limit, but the amplitude and velocity already strongly decreases before reaching it, so that the point at which the propagation stops is actually very close to $\rho=\rho_E$. Behind the pulse, a long recovery time is necessary for the core to be sufficiently replenished with fresh reactants for the system to be excitable again. Actually, fast diffusion of H^+ and OH^- restore the alcaline character of the core before this process is achieved, so that the restoring time is controled by the slow diffusion coefficient. The F/FT interface recedes, leaving the system in the F state but, since the F state cannot propagate into a stable FT state, it cannot deeply penetrate into the bistable domain so that the backwave stops at a ρ value close to the bistability limit. Afterwards, the system becomes again excitable and a new excitation wave starts. The process repeats periodically with a period T of the order of magnitude of the replenish time of the core in the vicinity of this starting point. For $r\sim0.5$ mm one has $T\sim r^2/D=250$ s. The real value is $T=246$ s. In fact, there is an apparent ambiguity on the point where the backwave stops, defining the starting point. Strictly speaking, this limit should be $\rho=\rho_B$. Yet, for $\rho_B<\rho<\rho_O$—i.e., $r_B<r<r_O$—one knows that, in the cylinder, the FT state is affected by oscillations of a different nature, which already indicates an instability of the FT state. In the strip or the cylinder, the width of the boundary layer which separates the acid core from the alcaline boundary oscillates in time. The closer the maximum width of this layer is from the depth l (strip) or the cylinder radius, i.e., the closer to the FT$\rightarrow$T transition, the larger is the amplitude and the period of these oscillations. One expects that, in the cone, this transverse instability can create a particular sensitivity of the FT state to the backwave. It occurs that, in our computation, this backwave goes up to a value close to $\rho=\rho_O$. Besides, a finer analysis shows that

these oscillations of the boundary layer slightly modulate the signal of the backwave in the vicinity of the CSTR boundaries. Nevertheless, this modulation remains small, since in the domain where these layer oscillations could become large in the cylinder, their period increases to values much larger than T, so that the longitudinal oscillations caused by the changes of r dominate and they determine the amplitude and frequency.

V. CONCLUSIONS

This work has been initiated in rapport with the development of a new field of research, namely chemomechanics, which associates chemical dissipative structures with chemosensitivity of soft matter (see Chaps. 3–8 in Ref. [23]). In particular, the search for rhythms and forms that could spontaneously emerge from the sole coupling between a reaction that exhibits bistability properties but no autonomous oscillations —like the CT reaction —and a chemoresponsive gel. Both for technical and fundamental reasons, the experiments make use of cylinders of gel of small radius, for which a number of crucial parameters cannot be measured directly.

We have rebuild a diagram of spatial bistability and excitability for the CT reaction in cylindrical geometry. One expects that the results can be extrapolated to the experimental data with the same degree of confidence as we have for the flat strip. It is impossible, in the cylindrical geometry, to evaluate experimentally the distribution of concentration in the radial direction, but our diagram allows to evaluate the corrections to the flat strip case, in particular the shift of the bistability and excitability limits to less alcaline CSTR states. But the most important point is that the computed diagram gives the r_B and r_E limits in the domain where they are small. The knowledge of these limits is extremely important in the search for chemomechanical motions that rely on spatial bistability since large changes of compositions occur at these precise sizes, inducing in turn a feedback on the geometry [19]. These data seem presently inaccessible in experiments on true cylinders.

It has been shown [15] that it was possible to study experimentally the dynamics in a conical gel. Here, we have made quantitative simulations on these dynamics and clarified their relations to the geometrical characteristics of the system. Let us remind an important point: The excitability and the oscillations along the axis of the cone do not find their origin in the sole reaction-diffusion process like in the classical oscillatory or excitable reactions, but are closely linked to the size of the system that controls the feeding in fresh reactants, an essential point for chemomechanics. The dynamics in the cone is due to the gradient of the size r along the axis. In our simulations, we have shown that, if necessary, a one shot experiment in the cone allows to determine quantitatively the essential parameters of the CT spatial bistability in the cylinder for a given state of the CSTR (i.e., a given value of $[OH^-]_0$). Actually, we show that the diffusion along the cone axis does not modify significantly the limits that could be predicted from naive arguments that neglects this diffusion. The turning point of the direct wave allows for an accurate determination of ρ_E, thus r_E. The turning point of the back wave allows for the determination of ρ_O, thus r_O. The problem we raised about the ambiguity that could remain between r_B and r_O is not of practical importance, since in small size systems, these values are always close to each other.

Thus, the results reported in this paper provide two different ways to access to the spatial bistability properties in cylindrical geometry at low radii. Taking the validity of the model in the flat strip case for granted, one can use the numerical simulations in cylindrical geometry. For a complementary or alternative experimental approach, one can perform a few experiments in a conical gel.

ACKNOWLEDGMENTS

We thank P. De Kepper, F. Gauffre, V. Labrot, and E. Dulos for numerous discussions and communication of experimental results. This work was supported by CNRS, Région Aquitaine, and the computation pole M3PEC of Bordeaux 1 University.

[1] Á. Tóth, I. Lagzi, and D. Horváth, J. Phys. Chem. **100**, 14837 (1996).
[2] D. Horváth and Á Tóth, J. Chem. Phys. **108**, 1447 (1998).
[3] M. Fuentes, M. N. Kuperman, and P. De Kepper, J. Phys. Chem. **105**, 6769 (2001).
[4] J. Boissonade, E. Dulos, F. Gauffre, M. Kuperman, and P. De Kepper, Faraday Discuss. **120**, 353 (2001).
[5] M. Fuentes, M. N. Kuperman, J. Boissonade, E. Dulos, F. Gauffre, and P. De Kepper, Phys. Rev. E **66**, 056205 (2002).
[6] T. Bánsági Jr., D. Horváth, Á. Tóth, J. Yang, S. Kalliadasis, and A. De Wit, Phys. Rev. E **68**, 055301 (2003).
[7] T. Bánsági Jr., D. Horváth, and Á. Tóth, Phys. Rev. E **68**, 026303 (2003); T. Bánsági Jr., D. Horváth, and Á. Tóth, Chem. Phys. Lett. **384**, 153 (2004).
[8] F. Gauffre, V. Labrot, J. Boissonade, and P. De Kepper, in Ref. [23].
[9] Z. Noszticzius, W. Horsthemke, W. D. McCormick, H. L. Swinney, and W. Y. Tam, Nature (London) **329**, 619 (1987).
[10] W. Y. Tam, Z. Noszticzius, W. Horsthemke, W. D. McCormick, and H. L. Swinney, J. Chem. Phys. **88**, 3395 (1988).
[11] B. Rudovics, E. Barillot, P. W. Davies, E. Dulos, J. Boissonade, and P. De Kepper, J. Phys. Chem. A **103**, 1790 (1999).
[12] K. J. Lee, D. McCormick, Q. Ouyang, and H. Swinney, Science **261**, 192 (1993).
[13] P. W. Davies, P. Blanchedeau, E. Dulos, and P. De Kepper, J. Phys. Chem. A **102**, 8236 (1998).
[14] P. Blanchedeau, J. Boissonade, and P. De Kepper, Physica D **147**, 283 (2000).
[15] F. Gauffre, V. Labrot, J. Boissonade, P. De Kepper, and E.

Dulos, J. Phys. Chem. A **107**, 4452 (2003).
[16] I. Nagypal and I. R. Epstein, J. Phys. Chem. **90**, 6285 (1986).
[17] P. Blanchedeau and J. Boissonade, Phys. Rev. Lett. **81**, 5007 (1998).
[18] M. Bachir, P. Borckmans, and G. Dewel, Phys. Rev. E **59**, R6223 (1999).
[19] J. Boissonade, Phys. Rev. Lett. **90**, 188302 (2003).
[20] P. Borckmans, K. Benyaich, and G. Dewel, Int. J. Quantum Chem. **98**, 239 (2004).
[21] V. S. Zykov, *Simulation of Wave Processes in Excitable Media* (Manchester University Press, Manchester, 1987).
[22] A. Mikhailov, *Foundations of Synergetics I. Distributed Active Systems* (Springer, Berlin, 1994).
[23] *Nonlinear Dynamics in Polymeric Systems*, ACS Symposium Series 869, edited by J. Pojman and Qi. Tran-Cong-Miyata (American Chemical Society, Washington, D.C., 2003).